The Chemical Shift Anisotropy: A Promising Parameter To Distinguish The 29 Si NMR Peaks In Zeolites

Eddy Dib, Svetlana Mintova, Georgi Vayssilov, Hristiyan Aleksandrov, Marina Carravetta

The Chemical Shift Anisotropy: A Promising Parameter To Distinguish The ^{29}Si NMR Peaks In Zeolites

Eddy Dib*[a,b], Svetlana Mintova[a], Georgi N. Vayssilov[c], Hristiyan A. Aleksandrov[c], Marina Carravetta*[b]

[a]Laboratoire Catalyse et Spectrochimie (LCS), Normandie University, ENSICAEN, CNRS, 6 boulevard du Marechal Juin, 14050 Caen, France

[b]School of Chemistry, University of Southampton, SO17 1BJ, United Kingdom

[c]Faculty of Chemistry and Pharmacy, University of Sofia, 1126 Sofia, Bulgaria

***KEYWORDS**: Solid-state NMR, DFT calculation, recoupling, zeolites*

ABSTRACT: Using a combination of (i) symmetry-based recoupling in ^{29}Si NMR, (ii) spin dynamics-based simulations and (iii) DFT-based theoretical calculations, we show how the ^{29}Si NMR peaks of (≡Si-O-Si≡) (Q^4(0Al)), Brønsted acid sites (≡Si-OH-Al≡) (Q^4(1Al)), and silanols (≡Si-OH) (Q^3), can be characterized in nanosized ZSM-5 zeolites. Significant differences in the chemical shift anisotropy are calculated theoretically and observed experimentally for silicon nuclei close to aluminum (Q^4(1Al)) comparing to those who are not i.e. Q^4(0Al) and Q^3, allowing one to clearly assign the ^{29}Si NMR peaks. The isotropic chemical shift alone cannot resolve such differences.

Introduction

Identification of the position and strength of acid sites is of paramount importance for solid state acid catalysis[1]. Tuning the location of acid sites in zeolites – extremely important catalysts and adsorbents in chemical industry – would allow the control of their acidity to enhance the yield of a specific reaction[2]. However, identifying the distribution of heteroatoms is challenging. Different experimental methods are used for their localization, either spectroscopic methods, including Nuclear Magnetic Resonance (NMR) and Infrared, or diffraction-based methods (electrons, neutrons and X-rays)[3]. These techniques are reaching their limits in terms of resolution and sensitivity, and continuous efforts are made to overcome the existing limitations[4]. Zeolites are ideal systems for NMR investigation, due to the natural presence of many nuclei in their skeletons which have an NMR active isotope (^{29}Si, ^{27}Al, ^{1}H, ^{17}O)[5]. NMR provides insight on atomic-scale organization and is ideally suited to study solids lacking long-range order. Magic-angle spinning (MAS) NMR, with rapid sample rotation about an axis at the angle $\beta_m = \arctan\sqrt{2}$ with respect to the main magnetic field, leads to spectra with higher resolution, averaging out the anisotropic interactions in solids[6]. In the pioneering works of Engelhardt and co-workers, silicon sites differing in their coordination state[7] were assigned through the increase in the ^{29}Si isotropic chemical shift, according to the number of tetrahedral atoms (T) in its vicinity, following the trend: Si(4Si), Si(3Si,1T), Si (2Si,2T), Si (1Si,3T), and Si (4T). The Q^n(mT) building units were defined as SiO_4 groups connected via oxygen bridges to m T and (n-m) other Si atoms, where n = 0 – 4 and m≤n. These studies resulted in many structural-spectroscopic correlations with either Si-O-Si, Si-O-T angles or Si-Si distances, allowing a clear understanding of zeolites structures[8–10].

The isomorphic substitution of Si by Al in the skeletons of zeolites is possible due to the similarities in size and electron density of both atoms, but their distinction by diffraction techniques is not trivial, especially when complex structures with many non-equivalent crystallographic sites are examined, allowing the introduction of new NMR methodologies to investigate the Al distribution using NMR such as ^{29}Si-^{27}Al HMQC-D experiments combined with DFT calculations[11].

The development of such methodologies in the last decades have contributed to the assignment of the experimental spectra, giving rise to the palette of techniques referred to as 'NMR crystallography'[12,13]. While the ^{29}Si NMR isotropic chemical shift is one of the most important NMR parameters for zeolites[14], the partial overlap of signals corresponding to different coordination states is a common problem hindering precise assignments[5,15] and chemical shift anisotropy was used to distinguish different Q^4(0Al) ^{29}Si environments in siliceous zeolites previously[16,17].

In this work, we show that chemical shift anisotropy (CSA) provides a promising parameter to distinguish ^{29}Si NMR signals of Q^4 species, being either Q^4(0Al) or Q^4(1Al) (Brønsted acid sites) and silanols in zeolites. DFT based energy minimization using CASTEP package[18] on ZSM-5 zeolite revealed a high CSA for the silicon sites adjacent to Al (Q^4(1Al)), compared to all other (Q^4(0Al)) sites and silanols present in the structure.

Synthesis

The nanosized ZSM-5 zeolite was synthesized using a clear precursor suspension with the following chemical composition: 0.25 TPAOH: 0.05 Na_2O: 0.0125 Al_2O_3: 1 SiO_2: 25 H_2O. For the preparation of the suspensions, the total amounts of double distilled water and organic structure directing agent (tetra n-propylammonium hydroxide (TPAOH), 20 wt. % in water solution, Alfa Aesar) were mixed for about 15 minutes using magnetic stirring. Then, the silicon source (tetraethyl orthosilicate (TEOS) 98%, Aldrich) was added dropwise to the suspension and subjected to magnetic stirring for one hour. Finally, the aluminum source (aluminum nitrate (Al $(NO_3)_3.9H_2O$, 97%, Prolabo) was added to the suspension followed by aging on an orbital shaker for 18 h at room temperature. Then, the hydrothermal treatment was carried out in Teflon-lined stainless-steel autoclaves at 180 °C for 72 h under autogenous pressure. The solids were purified with double-distilled water and high-speed centrifugation, until the pH of the supernatant was below 8. The samples were dried at 90 °C and calcined at 550 °C/5h in air.

Nuclear Magnetic Resonance

NMR measurements were performed on a 9.4 T Bruker magnet with a Bruker Neo console using a 5 mm PhoenixNMR triple resonance probe used in double resonance mode, with zirconium oxide pencil-style rotors fully packed of freshly calcined sample. Sample rotation was controlled using an A2B box. Experiments were acquired with a sample rotation of 7400 Hz, 20 s repetition delay. The data reported in **Figure 3** were acquired with the pulse sequence shown in Figure S1, they were obtained with 160 scans, 20 t1 increments with a step of 210.2 µs, which is equivalent to a set of 14 R-elements. For the recoupling sequence and for the detection pulses, a nutation frequency of $\omega_{nut}/2\pi$=18.5 kHz was used. The ^{29}Si axis was calibrated using tetramethylsilane as indirect reference[19].

Theoretical calculations

When applied to crystals, Density Functional Theory (DFT) calculations were done using CASTEP package version 20.1.1.[18,20] The principal components of the absolute shielding tensors, σ, and the corresponding isotropic shieldings, $\sigma_{iso} = (1/3)\,Tr\{\sigma\}$, were calculated for ^{29}Si nuclei after optimization of the atomic positions and unit cell parameters. The MFI structure optimized corresponds to the $P2_1/n$ symmetry[21,22] (24 T sites), the input CIF file was downloaded from the IZA website[23]. The relationship between the experimental isotropic chemical shifts and the calculated isotropic shieldings is given by $\sigma_{iso} = -0.69\,\delta_{iso} + 193.3$. This relationship is in line with the one published by Dawson et al. recently ($\delta_{iso} = -0.73\,\sigma_{iso} + 211.79$)[14]. The calculations applied to clusters were done using ORCA package[24]. They are detailed in the supporting information (section S2).

Results and discussion

Figure 1 shows the results from CASTEP calculations (see section S2 in SI). The distribution of the calculated CSA against the corresponding isotropic chemical shielding, σ_{iso}, are displayed. The CSA is defined following Haeberlen convention as the difference between the zz-component of the chemical shift tensor in its principal axis frame and the corresponding σ_{iso}, namely $\sigma_{aniso} = (\sigma_{zz} - \sigma_{iso})$.[25]
Calculations were performed for silicalite-1 and ZSM-5 zeolites that consist of (24 Si) sites and (23 Si + 1 Al) respectively considering the Al in the 24 possible T positions (T1 – T24). The differences observed for all sites are always the same (average CSA (Q^4(1Al)) are approximatively four times higher than the CSA (Q^4(0Al)), the results are presented in Table S1. ZSM-5 crystals with Al in T1 and T24 are the only ones presented in **Figure 1** for clarity. Although both structures (silicalite-1 and ZSM-5) belong to the same MFI (Mobil Five) topology, the strength of anisotropy is only pronounced for the Si sites adjacent to Al in ZSM-5 (average CSA of 48.8 ppm). All the remaining Q^4 sites in both silicalite-1 and ZSM-5 have a lower CSA (average CSA of 12.4 ppm). The values obtained here for the Q^4(0Al) sites are in line with the ones published earlier by Brouwer et al.[26] presenting an average CSA of 10 ppm.

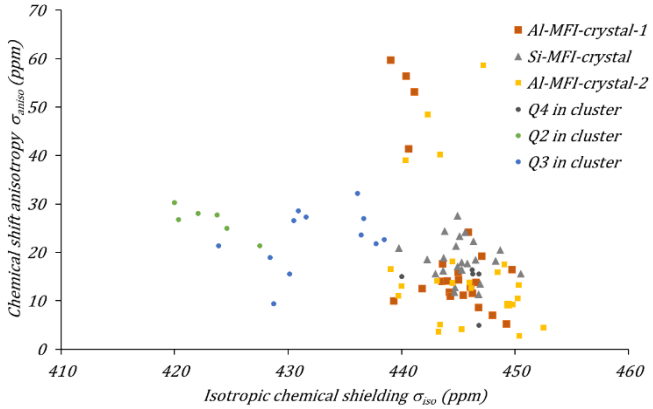

Figure 1. Calculated chemical shift anisotropies (CSA) vs. isotropic chemical shieldings (σ_{iso}), for silicalite-1, ZSM-5 and clusters of MFI with different configurations of silanols.

The four silicon sites adjacent to Al are among the lowest chemical shielded sites as expected, but they are not the only ones exhibiting this isotropic chemical shielding. To ensure the large CSA is specifically due to the presence of Al in the structure, we considered different clusters of MFI with and without Al, optimized with ORCA package,[24] with several configurations of silanols (isolated and hydrogen bonded, see Figure S2 and Table S4, section S2.2 in SI). **Figure 1** shows the CSA dependence with respect to σ_{iso} for the corresponding silanols either in Q^2 or Q^3 coordination in addition to the Q^4 sites present in the cluster, while the isotropic chemical shieldings follows the expected trend σ_{iso} (Q^4) > σ_{iso} (Q^3) > σ_{iso} (Q^2), the CSA does not exceed 30 ppm, with an average CSA of 21 ppm. These results permit to distinguish the ^{29}Si signals of silanols from those of Brønsted acid sites convincingly (see Section S2 and Tables S1-S6). The CSA of Si-O-Al sites are higher than all other CSA of Q^4 sites and silanols in the considered models. However, we have to mention that the silanols configurations in the clusters may be distorted in various ways in the final angular configurations considering the size of the cluster. In other disordered structures examined by Hedin et al.[27], Q^4(0Al)showed an anisotropy of 10 ppm, in line with our results while silanols exhibited high

CSA values i.e. 40 and 60 ppm, this may be explained by a strong angular distortions as it was recently shown using a local geometry descriptor for ^{29}Si CSA[28].

The theoretical prediction was validated by NMR measurements of the CSA on a well-ordered ZSM-5 nanosized zeolite with a Si/Al = 40, and described in details elsewhere[29]. This model sample has a high resolution in the Q^4(0Al) sites and a small amount of Q^4(1Al) sites (**Figure 2**). From previous work[30], the amount of structural defects (SiOH) in this sample is negligible compared to Bronsted acid sites and they are mainly free silanols, see the IR spectrum (Figure S3 in SI). Then, the peak at -106 ppm is mainly assigned to the presence of Al. Even for an equal amount of SiOH and SiOHAl groups, we expect 1Si as Q3 vs. 4Si as Q4(1Al)). Furthermore, we have recorded a ^{27}Al-^{29}Si HMQC-D spectrum (not shown here) to ensure that the peak at -106 ppm could be assigned to SiOAl groups. The direct determination of the CSA through the study of the spinning sideband pattern is not possible at high MAS frequency, because the CSA is averaged out by MAS[31] at the rotation speeds considered here. MAS is essential to provide spectra with sufficient resolution to discriminate the different chemical environments for ^{29}Si in these samples. To gain access to the anisotropic interactions that give insights about structural features in solids, recoupling techniques can be used[32]. The symmetry-based recoupling sequence $R18_2^5$ sequence was selected here for CSA recoupling (see section S1 and Figure S1), to reintroduce the CSA in the second dimension of a two-dimensional NMR spectrum[33].

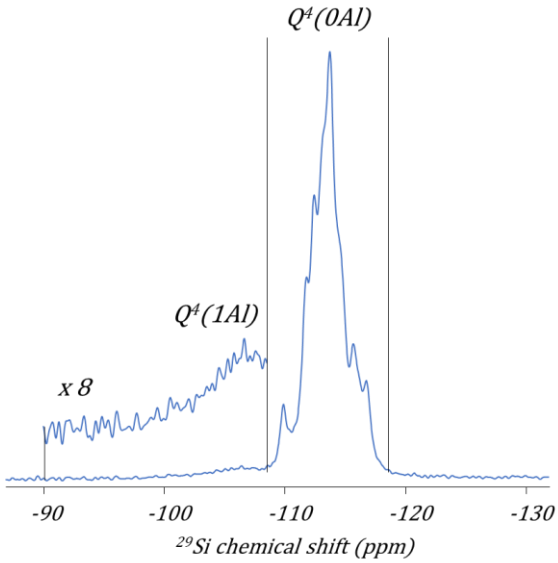

Figure 2. ^{29}Si NMR spectrum of nanosized ZSM-5 acquired using direct acquisition at 9.4 Tesla in a 5 mm rotor spinning at 9 kHz with a recycle delay of 20 s.

This approach was successfully demonstrated in literature[34], including ^{1}H NMR[33] and ^{19}F NMR studies[35]. Despite its low sensitivity toward asymmetry parameters, this method was selected here to estimate the strength of the CSA coupling only, knowing the potential overlapping of 4 Q^4(1Al) Si sites for every Al position in the framework in addition to the low amount of Al in the sample (Si/Al = 40). The $R18_2^5$ sequence consists of a continuous series of 180° pulses that alternate in phase by ±50° synchronized such that 18 pulses (9 pairs) are applied during two sample rotational periods about the magic-angle. According to the selection rules derived from average Hamiltonian theory[36], it recouples selectively the CSA, the heteronuclear dipolar interactions, as well as homonuclear J-coupling interactions and suppresses other anisotropic interactions like homonuclear dipolar interactions, isotropic chemical shifts and heteronuclear J-coupling interactions. Thanks to the negligible amount of silanols in our sample and to the high resolution of the Q^4(0Al) sites, the line shapes obtained in the indirect dimension of the 2D anisotropic-isotropic chemical shift correlation experiment after Fourier transformation reflects the magnitude of the CSA interaction (**Figure 3**). The splitting observed reflects the strength of the CSA for each site. The higher the CSA, the wider the splitting between the peaks in the recoupling dimension.

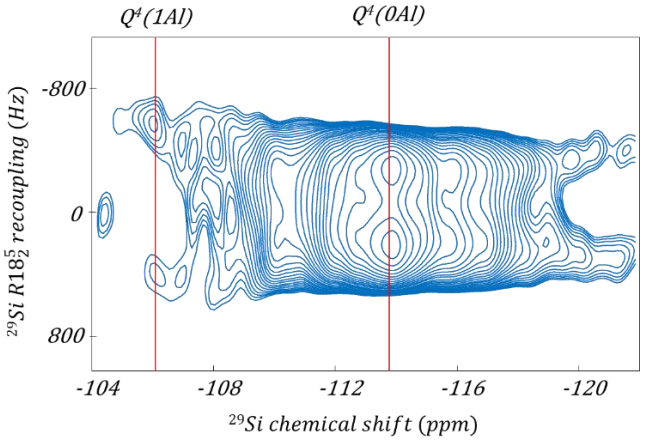

Figure 3. 2D ^{29}Si anisotropic-isotropic chemical shift correlation spectrum of ZSM-5 zeolite obtained at 7.4 kHz MAS frequency using the $R18_2^5$ sequence.

To extract the CSA from the experimental data, we have considered two slices (indicated by the red dotted lines in **Figure 3**) corresponding to Q^4(1Al) and Q^4(0Al) sites at -106 and -114 ppm respectively. **Figure 4** shows the comparison between the selected experimental slices and the corresponding simulations, using the Simpson software package[37]**.** The CSA used for the simulations are σ_{aniso}(Q^4(1Al))= 50.0 ppm and σ_{aniso}(Q^4(0Al))= 16 ppm, which agree remarkably well with the average values from CASTEP of 48.8 ppm and 12.4 ppm respectively.

Simulations were performed using 986 alpha-beta angles according to the ZCW scheme[38]. A chemical shift asymmetry, $\eta = 0$, in both cases, a ^{27}Al-^{29}Si heteronuclear dipolar coupling of 230 Hz and a ^{27}Al quadrupolar coupling of 3 MHz were considered for Q^4(1Al). Their effect is not very pronounced on the spacing observed in the patterns despite their effects on the sharpness of the doublet (Figure S4).

The differences observed reflect the high geometric distortion within the Q^4(1Al) sites compared to all Q^4(0Al) sites, in line with a recently proposed local geometry descriptor for the CSA coupling in ^{29}Si NMR[28].

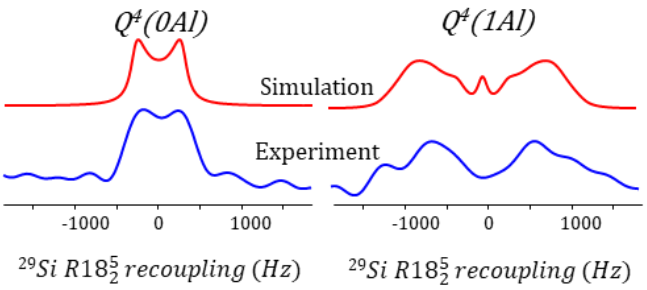

Figure 4. Experimental ^{29}Si CSA recoupled line shapes obtained from slices of **Figure 3** corresponding to Q^4(1Al) (−106 ppm) and Q^4(0Al) (−114 ppm) sites and associated SIMPSON simulations, using $\sigma_{aniso}(Q^4(1\text{Al})) = 50.0$ ppm, $\sigma_{aniso}(Q^4(0\text{Al})) = 16$ ppm and $\eta = 0$ for both sites.

Conclusion

In conclusion, this work provides a new promising approach using ^{29}Si NMR spectroscopy to distinguish certain overlapping signals i.e. Q^4(0Al) and Q^4(1Al) and probe the presence of heteroatoms in zeolites (Al in this case). It opens the door for further developments and allows the extension of the use of ^{29}Si NMR spectroscopy to locate and understand better the distribution of heteroatoms in zeolites.

ASSOCIATED CONTENT

Details about the synthesis of the zeolite, the NMR experiments and the theoretical calculations are supplied as Supporting Information. This material is available free of charge via the Internet at http://pubs.acs.org."

AUTHOR INFORMATION

Corresponding Authors

* eddy.dib@ensicaen.fr ; m.carravetta@soton.ac.uk

Author Contributions

The manuscript was written through contributions of all authors. All authors have given approval to the final version of the manuscript.

ACKNOWLEDGMENT

We acknowledge the support of the Label of Excellence for the Centre for zeolites and nanoporous materials by the Region of Normandy (CLEAR) and the International Exchange program of the Royal Society of Chemistry, grant number IES\R3\213078. We also acknowledge the use of the IRIDIS High Performance Computing Facility, and associated support services at the University of Southampton, in the completion of this work. Prof. Malcolm H. Levitt and Prof. Ilya Kuprov are acknowledged for stimulating discussions.

REFERENCES

(1) Corma, A. Solid Acid Catalysts. *Curr. Opin. Solid State Mater. Sci.* **1997**, *2* (1), 63–75. https://doi.org/10.1016/S1359-0286(97)80107-6.

(2) Pinar, A. B.; Gómez-Hortigüela, L.; McCusker, L. B.; Pérez-Pariente, J. Controlling the Aluminum Distribution in the Zeolite Ferrierite via the Organic Structure Directing Agent. *Chem. Mater.* **2013**, *25* (18), 3654–3661. https://doi.org/10.1021/cm4018024.

(3) Medeiros-Costa, I. C.; Dib, A. E.; Nesterenko, N.; Dath, J.-P.; Gilson, J.-P.; Mintova, S. Silanol Defect Engineering and Healing in Zeolites: Opportunities to Fine-Tune Their Properties and Performances. *This J. is Cite this Chem. Soc. Rev* **1115**, *50*, 11156. https://doi.org/10.1039/d1cs00395j.

(4) Schroeder, C.; Siozios, V.; Hunger, M.; Hansen, M. R.; Koller, H. Disentangling Brønsted Acid Sites and Hydrogen-Bonded Silanol Groups in High-Silica Zeolite H-ZSM-5. *J. Phys. Chem. C* **2020**, *124* (42), 23380–23386. https://doi.org/10.1021/acs.jpcc.0c06113.

(5) Koller, H.; Weiß, M. Solid State NMR of Porous Materials: Zeolites and Related Materials. *Top. Curr. Chem.* **2012**, *306*, 189–228. https://doi.org/10.1007/128_2011_123.

(6) Polenova, T.; Gupta, R.; Goldbourt, A. Magic Angle Spinning NMR Spectroscopy: A Versatile Technique for Structural and Dynamic Analysis of Solid-Phase Systems. *Anal. Chem* **2015**, *87*, 34. https://doi.org/10.1021/ac504288u.

(7) Engelhardt, G. Multinuclear Solid-State NMR in Silicate and Zeolite Chemistry. *Trends Anal. Chem*. Elsevier October 1, 1989, pp 343–347. https://doi.org/10.1016/0165-9936(89)87043-8.

(8) Engelhardt, G.; Radeglia, R. A Semi-Empirical Quantum-Chemical Rationalization of the Correlation between SiOSi Angles and 29Si NMR Chemical Shifts of Silica Polymorphs and Framework Aluminosilicates (Zeolites). *Chem. Phys. Lett.* **1984**, *108* (3), 271–274. https://doi.org/10.1016/0009-2614(84)87063-3.

(9) S. Ramdas & J. Klinowski. A Simple Correlation between Isotropic 29Si-NMR Chemical Shifts and T–O–T Angles in Zeolite Frameworks. *Nat. 1984 3085959* **1984**, *308* (5959), 521–523. https://doi.org/10.1038/308521a0.

(10) Engelhardt, G.; Luger, S.; Buhl, J. C.; Felsche, J. 29Si MAS n.m.r. of Aluminosilicate Sodalites: Correlations between Chemical Shifts and Structure Parameters. *Zeolites* **1989**, *9* (3), 182–186. https://doi.org/10.1016/0144-2449(89)90023-7.

(11) Dib, E.; Mineva, T.; Veron, E.; Sarou-Kanian, V.; Fayon, F.; Alonso, B. ZSM-5 Zeolite: Complete Al Bond Connectivity and Implications on Structure Formation from Solid-State NMR and Quantum Chemistry Calculations. *J. Phys. Chem. Lett.* **2018**, *9* (1), 19–24. https://doi.org/10.1021/acs.jpclett.7b03050.

(12) Brouwer, D. H.; Darton, R. J.; Morris, R. E.; Levitt, M. H. A Solid-State NMR Method for Solution of Zeolite Crystal Structures. *J. Am. Chem. Soc.* **2005**, *127* (29), 10365–10370. https://doi.org/10.1021/JA052306H/SUPPL_FILE/JA052306HSI20050526_112405.PDF.

(13) Martineau, C. NMR Crystallography: Applications to Inorganic Materials. *Solid State Nucl. Magn. Reson.* **2014**, *63–64*, 1–12. https://doi.org/10.1016/J.SSNMR.2014.07.001.

(14) Dawson, D. M.; Moran, R. F.; Ashbrook, S. E. An NMR Crystallographic Investigation of the Relationships

between the Crystal Structure and 29Si Isotropic Chemical Shift in Silica Zeolites. *J. Phys. Chem. C* **2017**, *121* (28), 15198–15210. https://doi.org/10.1021/ACS.JPCC.7B03730/ASSET/IMAGES/LARGE/JP-2017-037309_0009.JPEG.

(15) Brouwer, D. H. Applications of Silicon-29 NMR Spectroscopy. *Compr. Inorg. Chem. III* **2023**, 107–137. https://doi.org/10.1016/B978-0-12-823144-9.00032-7.

(16) Brouwer, D. H.; Enright, G. D. Probing Local Structure in Zeolite Frameworks: Ultrahigh-Field NMR Measurements and Accurate First-Principles Calculations of Zeolite 29Si Magnetic Shielding Tensors. *J. Am. Chem. Soc.* **2008**, *130* (10), 3095–3105. https://doi.org/10.1021/ja077430a.

(17) Brouwer, D. H. NMR Crystallography of Zeolites: Refinement of an NMR-Solved Crystal Structure Using Ab Initio Calculations of 29Si Chemical Shift Tensors. *J. Am. Chem. Soc.* **2008**, *130* (20), 6306–6307. https://doi.org/10.1021/ja800227f.

(18) Clark, S. J.; Segall, M. D.; Pickard, C. J.; Hasnip, P. J.; Probert, M. I. J.; Refson, K.; Payne, M. C. First Principles Methods Using CASTEP. *Zeitschrift fur Krist.* **2005**, *220* (5–6), 567–570. https://doi.org/10.1524/ZKRI.220.5.567.65075/MACHINEREADABLECITATION/RIS.

(19) Hayashi, S.; Hayamizu, K. Chemical Shift Standards in High-Resolution Solid-State NMR (1) 13 C, 29 Si, and 1 H Nuclei . *Bull. Chem. Soc. Jpn.* **1991**, *64* (2), 685–687. https://doi.org/10.1246/BCSJ.64.685.

(20) Yates, J. R.; Pickard, C. J.; Mauri, F. Calculation of NMR Chemical Shifts for Extended Systems Using Ultrasoft Pseudopotentials. *Phys. Rev. B - Condens. Matter Mater. Phys.* **2007**, *76* (2), 024401. https://doi.org/10.1103/PHYSREVB.76.024401/FIGURES/2/MEDIUM.

(21) van Koningsveld, H.; Jansen, J. C.; van Bekkum, H. The Monoclinic Framework Structure of Zeolite H-ZSM-5. Comparison with the Orthorhombic Framework of as-Synthesized ZSM-5. *Zeolites* **1990**, *10* (4), 235–242. https://doi.org/10.1016/0144-2449(94)90134-1.

(22) Fyfe, C. A.; Grondey, H.; Feng, Y.; Kokotailo, G. T. Investigation of the Three-Dimensional Si□O□Si Connectivities in the Monoclinic Form of Zeolite ZSM-5 by Two-Dimensional 29Si INADEQUATE Experiments. *Chem. Phys. Lett.* **1990**, *173* (2–3), 211–215. https://doi.org/10.1016/0009-2614(90)80080-W.

(23) *Database of Zeolite Structures*. http://www.iza-structure.org/databases/ (accessed 2022-12-09).

(24) Neese, F.; Wiley, J. The ORCA Program System. *Wiley Interdiscip. Rev. Comput. Mol. Sci.* **2012**, *2* (1), 73–78. https://doi.org/10.1002/WCMS.81.

(25) Harris, R. K.; Becker, E. D.; Cabral De Menezes, S. M.; Granger, P.; Hoffman, R. E.; Zilm, K. W. Further Conventions for NMR Shielding and Chemical Shifts (IUPAC Recommendations 2008). *Pure Appl. Chem.* **2008**, *80* (1), 59–84. https://doi.org/10.1351/PAC200880010059/MACHINEREADABLECITATION/RIS.

(26) Brouwer, D. H.; Enright, G. D. Probing Local Structure in Zeolite Frameworks: Ultrahigh-Field NMR Measurements and Accurate First-Principles Calculations of Zeolite 29Si Magnetic Shielding Tensors. *J. Am. Chem. Soc.* **2008**, *130* (10), 3095–3105. https://doi.org/10.1021/JA077430A/SUPPL_FILE/JA077430A-FILE003.CIF.

(27) Hedin, N.; Graf, R.; Christiansen, S. C.; Gervais, C.; Hayward, R. C.; Eckert, J.; Chmelka, B. F. Structure of a Surfactant-Templated Silicate Framework in the Absence of 3D Crystallinity. *J. Am. Chem. Soc.* **2004**, *126* (30), 9425–9432. https://doi.org/10.1021/JA040030S/ASSET/IMAGES/LARGE/JA040030SF00005.JPEG.

(28) Venetos, M. C.; Dwaraknath, S.; Persson, K. A. Effective Local Geometry Descriptor For29Si NMR Q4Anisotropy. *J. Phys. Chem. C* **2021**, *125* (35), 19481–19488. https://doi.org/10.1021/ACS.JPCC.1C04829/SUPPL_FILE/JP1C04829_SI_002.ZIP.

(29) Konnov, S. V.; Dubray, F.; Clatworthy, E. B.; Kouvatas, C.; Gilson, J.; Dath, J.; Minoux, D.; Aquino, C.; Valtchev, V.; Moldovan, S.; Koneti, S.; Nesterenko, N.; Mintova, S. Novel Strategy for the Synthesis of Ultra-Stable Single-Site Mo-ZSM-5 Zeolite Nanocrystals. *Angew. Chemie* **2020**, No. 59, 19553– 19560. https://doi.org/10.1002/ange.202006524.

(30) Medeiros-Costa, I. C.; Dib, E.; Dubray, F.; Moldovan, S.; Gilson, J. P.; Dath, J. P.; Nesterenko, N.; Aleksandrov, H. A.; Vayssilov, G. N.; Mintova, S. Unraveling the Effect of Silanol Defects on the Insertion of Single-Site Mo in the MFI Zeolite Framework. *Inorg. Chem.* **2022**, *61* (3), 1418–1425. https://doi.org/10.1021/ACS.INORGCHEM.1C03076/ASSET/IMAGES/LARGE/IC1C03076_0008.JPEG.

(31) Antzutkin, O. N.; Shekar, S. C.; Levitt, M. H. Two-Dimensional Sideband Separation in Magic-Angle-Spinning NMR. *J. Magn. Reson. Ser. A* **1995**, *115* (1), 7–19. https://doi.org/10.1006/JMRA.1995.1142.

(32) Levitt, M. H. Symmetry-Based Pulse Sequences in Magic-Angle Spinning Solid-State NMR. *eMagRes* **2007**, *2007*. https://doi.org/10.1002/9780470034590.EMRSTM0551.

(33) Brouwer, D. H.; Ripmeester, J. A. Symmetry-Based Recoupling of Proton Chemical Shift Anisotropies in Ultrahigh-Field Solid-State NMR. *J. Magn. Reson.* **2007**, *185* (1), 173–178. https://doi.org/10.1016/J.JMR.2006.12.003.

(34) Hou, G.; Byeon, I. J. L.; Ahn, J.; Gronenborn, A. M.; Polenova, T. Recoupling of Chemical Shift Anisotropy by R-Symmetry Sequences in Magic Angle Spinning NMR Spectroscopy. *J. Chem. Phys.* **2012**, *137* (13), 134201. https://doi.org/10.1063/1.4754149.

(35) Porat-Dahlerbruch, G.; Struppe, J.; Quinn, C. M.; Gronenborn, A. M.; Polenova, T. Determination of Accurate 19F Chemical Shift Tensors with R-Symmetry Recoupling at High MAS Frequencies (60–100 KHz). *J. Magn. Reson.* **2022**, *340*, 107227. https://doi.org/10.1016/J.JMR.2022.107227.

(36) Brinkmann, A. Introduction to Average Hamiltonian Theory. I. Basics. *Concepts Magn. Reson. Part A* **2016**, *45A* (6), e21414. https://doi.org/10.1002/CMR.A.21414.

(37) Bak, M.; Rasmussen, J. T.; Nielsen, N. C. SIMPSON: A General Simulation Program for Solid-State NMR Spectroscopy. *J. Magn. Reson.* **2000**, *147* (2), 296–330. https://doi.org/10.1006/JMRE.2000.2179.

(38) Edén, M. Computer Simulations in Solid-State NMR. III. Powder Averaging. *Concepts Magn. Reson. Part A* **2003**, *18A* (1), 24–55. https://doi.org/10.1002/CMR.A.10065.

SYNOPSIS TOC

^{29}Si Chemical shift anisotropy in solid-state NMR is a promising parameter to distinguish the ^{29}Si NMR peaks in zeolites.